Thermal localization as a potential mechanism to rift cratons

Gang Lu, [1,2,*] Boris J.P. Kaus [2,3], Liang Zhao [1]

[1] State Key Laboratory of Lithospheric Evolution, Institute of Geology and Geophysics, Chinese Academy of Sciences, Beijing, 100029, China

[2] Department of Earth Science, ETH Zurich, Sonneggstrasse 5, 8092 Zurich, Switzerland

[3] University of Southern California, Los Angeles USA.

* Corresponding author e-mail: lvgang@mail.iggcas.ac.cn, Fax: +86-10-62010846

Abstract

Cratons are cold regions of continents that have remained stable since at least the Precambrian. The longevity of cratons is often attributed to chemical buoyancy and/or high viscosity of cratonic root material. Yet examples of destructed cratons (such as the North China Craton) suggest that there are conditions under which chemical buoyancy and/or high viscosity are insufficient to keep cratons stable. The formation of continental rifts, as weak zones that reduce the total stresses of cratons, may be a mechanism that increases the longevity of cratonic lithosphere. Since continental rifts result from localized deformation, understanding the mechanism of shear localization is thus important for understanding the stability or breakup of cratons. Here, we perform 2-D numerical models for a cratonic lithosphere under extension to understand the initiation of shear localization, for visco-elasto-plastic rheologies. Results reveal that three modes of deformation exist: no localization, symmetric localization and asymmetric localization. To further understand the underlying physics, we develop a 1-D semi-analytical method that predicts the onset of localization as well as whether rifting will be symmetric or asymmetric. Applications of the semi-analytical method to geological settings show that fast deformation, cold thermal state or strong mantle rheology may result in localized deformation and stabilize the remaining adjacent cratons. Our results successfully interpret the major features of the North China Craton.

Keywords: thermal localization; numerical modeling; lithospheric thinning; North China Craton

1. Introduction

Archean cratons are regions of continents that have remained undeformed since at least the Precambrian. They are characterized by relatively low surface heat flow, diamond deposits in kimberlites, and thick keels with high seismic velocities. Most Archean cratons have undergone minimal internal deformation, despite being directly adjacent to orogens or rifts (e.g. the east African Rift System, the Baikal Rift) at their boundaries (e.g. Stern et al., 1994; O'Neill et al., 2008; Sengor, 1999).

Yet, there are examples showing that cratonic lithosphere can be destructed as well e.g. the Wyoming Craton and the North China Craton (NCC) (Eggler et al., 1988; Carlson et al., 2004; Fan & Menzies, 1992; Menzies et al., 1993; Griffin et al., 1998).

Although the longevity of cratonic lithosphere is often attributed to chemical buoyancy and/or high viscosity of cratonic root material (Shapiro et al., 1999; Sengor, 1999), they are relatively ineffective if cratons are involved with subduction zones (Lenardic et al., 2000,2003). The existence of weak mobile zones surrounding cratons, in addition, was proposed to be a possible mechanism to increase the longevity of cratonic lithosphere (Lenardic et al., 2000). Such weak zones could be continental rifts and orogens that have relatively low yield stresses. Once a weak zone is initiated, the integrated stress of the lithosphere would reduce significantly which keeps the remaining part of the craton relatively undeformed. This might explain why most cratons are stable, even though they are adjacent to rifts or orogens (O'Neill et al., 2008). The formation of continental rifts is due to lithospheric runaway in which deformation is strongly localized in narrows zones (e.g., England, 1983; Buck, 1991; Buck et al., 1999). While some authors (e.g. England, 1983; Buck et al., 1991) extended the concept of rifts to be narrow rifts or wide rifts, it is the narrow rifts that behave as weak zones and stabilize cratons. Wide rifts, in contrast, can be observed in destructed cratons, e.g. the eastern North China Craton (Zhao & Xue, 2010), and the West Siberia Basin (Armitage & Allen, 2010). They are thought to result from stretching of relatively thick continental lithosphere without shear localization (Armitage & Allen, 2010; Buck, 1991). Better understanding the mechanisms of localization is thus important to understand dynamics of continental evolution.

A number of studies have been focusing on the mechanisms of localization (e.g. Bercovici & Karato, 2003; Montesi & Zuber, 2002; and references therein). Dynamic mechanisms of self-softening are required to generate localization (Bercovici & Karato, 2003; Montesi and Zuber 2002). Proposed mechanisms include grain size reduction (Kameyama et al., 1997; Jin et al., 1998; Braun et al., 1999), grain boundary sliding (Precigout & Gueydan, 2009), two phase damage (Bercovici et al., 2001a; Bercovici et al., 2001b; Landuyt & Bercovici, 2009) with microcrack or void generation (Ashby & Sammis, 1990; Regenauer-Lieb, 1999), lattice preferred orientation of olivine (Tommasi et al., 2009), or shear heating (Schubert & Turcotte, 1972; Bercovici, 1996; Regenauer-Lieb & Yuen, 2004;). In this study we focus on the thermal feedback, the coupling of shear heating and temperature-dependent viscosity, as the softening mechanism. This process has been intensively studied over last decades (e.g. Braeck & Podladchikov, 2007; Kameyama et al., 1999; Ogawa, 1987; Burg & Schmalholz, 2008; Kaus & Podladchikov, 2006; Regenauer-Lieb et al., 2001; Schmalholz et al., 2009; Crameri & Kaus, 2010). One and two-dimensional models illustrated that this mechanism might indeed cause lithospheric-scale shear zones. Yet, because many parameters were involved, it was difficult to understand which of those were the key parameters. Therefore, Kaus and Podladchikov (2006) performed a systematical study and derived scaling laws for the onset of localization. The scaling law showed that the onset of localization is given by $\dot{\varepsilon}_{bg} \geq \frac{1.4}{\Delta L}\sqrt{\frac{\kappa \rho c_p}{\mu_{eff}\gamma}}$, where κ is the thermal diffusivity, μ_{eff} the effective viscosity and ΔL the heterogeneity length scale. $\gamma = E / nRT^2$ is the e-fold length of the viscosity. Crameri and Kaus (2010) further extended the parameter study by taking into account the rheological stratification of the lithosphere as well as non-linear power law rheologies for a lithosphere under compression. The 1-D models derived in this latter study were capable of predicting whether localization occurs or not. Yet, they typically predicted localization to initiate at smaller strains than observed in 2-D numerical simulations. Here, we improve this and propose a new semi-analytical model to predict the onset of shear localization under extensional boundary conditions. The semi-analytical model is compared with numerous 2-D numerical simulations that model a thick lithosphere with Earth-like rheology and stratification under pure-shear extension. The 2-D simulations reveal three distinct modes of deformation, namely (1) the no localization mode, (2) the symmetric localization mode, and (3) the asymmetric localization mode. It is demonstrated that the semi-analytical model is capable of predicting the occurrence of localization, including whether rifting is symmetric or asymmetric. In a next step, we use our results to speculate on the causes of the breakup of the NCC.

2. Model setup

2.1 Mathematical Equations

The incompressible Boussinesq equations for a slowly deforming lithosphere are given by

$$\frac{\partial v_i}{\partial x_i} = 0$$

$$\frac{\partial \sigma_{ij}}{\partial x_j} + \rho_0(1-\alpha(T-T_0))g_i = 0$$

$$\rho c_p\left(\frac{\partial T}{\partial t} + v_j\frac{\partial T}{\partial x_j}\right) = \frac{\partial}{\partial x_j}\left(k\frac{\partial T}{\partial x_j}\right) + H_r + H_s \qquad (1)$$

where v_i is the velocity, x_i the spatial coordinates, *t* the time, *T* the temperature, ρ the density, α the thermal expansivity, g_i the gravitational acceleration, $\sigma_{ij} = -P\delta_{ij} + \tau_{ij}$ the total stress, $P = -\sigma_{ii}/3$ the pressure, δ_{ij} the Kronecker delta, τ_{ij} the deviatoric stress, c_p the heat capacity, *k* the thermal conductivity, H_r *the* radioactive heat production, and $H_s = \tau_{ij}(\dot{\varepsilon}_{ij} - \frac{1}{2G}\frac{D\tau_{ij}}{Dt})$ the shear heating.

The strain rate is defined as

$$\dot{\varepsilon}_{ij} = \frac{1}{2}\left(\frac{\partial v_i}{\partial x_j} + \frac{\partial v_j}{\partial x_i}\right)$$

The rheology of rocks is Maxwell visco-elasto-plastic:

$$\dot{\varepsilon}_{ij} = \frac{\tau_{ij}}{2\mu} + \frac{1}{2G}\frac{D\tau_{ij}}{Dt} + \dot{\lambda}\frac{\partial Q}{\partial \sigma_{ij}}$$

$$\frac{D\tau_{ij}}{Dt} = \frac{\partial \tau_{ij}}{\partial t} + v_k \frac{\partial \tau_{ij}}{\partial x_k} - W_{ik}\tau_{kj} + \tau_{ik}W_{kj} \qquad (2)$$

where μ is the effective viscosity, G the elastic shear module, $\dot{\lambda}$ the plastic multiplier, Q the plastic flow potential and $W_{ij} = \frac{1}{2}(\frac{\partial v_i}{\partial x_j} - \frac{\partial v_j}{\partial x_i})$ the vorticity.

The creep rheology is strain rate and temperature dependent:

$$\mu = \frac{1}{2} A^{\frac{1}{n}} \dot{\varepsilon}_{2nd}^{\frac{1}{n}-1} \exp(\frac{E}{nRT}) \qquad (3)$$

where A is a pre-exponential parameter, n the power-law exponent, $\dot{\varepsilon}_{2nd} = (0.5\dot{\varepsilon}_{ij}\dot{\varepsilon}_{ij})^{0.5}$ the second invariant of the strain-rate tensor, E the activation energy and R the universal gas constant.

The brittle strength of crustal rocks is approximated by Mohr-Coulomb plasticity:

$$F = \tau^* - \sigma^* \sin(\phi) - C\cos(\phi)$$

$$Q = \tau^*$$

$$\dot{\lambda} \geq 0, F \leq 0, \dot{\lambda}F = 0 \qquad (4)$$

where $\tau^* = ((0.5(\sigma_{zz} - \sigma_{xx}))^2 + \sigma_{xz}^2)^{0.5}$, $\sigma^* = -0.5(\sigma_{xx} + \sigma_{zz})$, C cohesion and ϕ the internal angle of friction. For rocks in the mantle, the yield strength is described by "Peierls" or "low-temperature" plasticity. Here the formulation of Goetze and Evans (1979) is applied which is valid for differential stresses that are larger than 200 MPa:

$$\tau_{ij} = \frac{\dot{\varepsilon}_{ij}\sigma_0}{\sqrt{3}\dot{\varepsilon}_{2nd}}(1-\sqrt{\frac{RT}{H_0}\ln(\frac{\sqrt{3}E_0}{2\dot{\varepsilon}_{2nd}})}) \qquad (5)$$

with σ_0=8.5×10^9 Pa, E_0=5.7×10^{11} s^{-1} and H_0=525 kJ/mol.

2.2 The 2-D Model

Our standard 2-D setup is 800km wide by 670km deep (Figure 1). The model is laterally homogeneous and consists of an upper crust (25km), a lower crust(15km), a mantle lithosphere(150km) and asthenosphere mantle(480km) (see table 1 for model parameters). The whole model with a free surface is subjected to pure shear extension with prescribed extensional strain rate $\dot{\varepsilon}_{bg}$. The thermal boundary conditions are zero-flux at side boundaries and isothermal at the top (0 °C) and the bottom (1600 °C) boundaries. The steady-state initial temperature is obtained by performing half-space cooling from 1600 °C to 0 °C at the surface over a time thermal age. The deep part of the mode, where temperature is greater than 1300 °C, is replaced by an adiabatic temperature gradient of 0.5 °C /km. Deviatoric stresses are initially zero. The extensional strain rate is varied from 10^{-16} to 10^{-13} s^{-1}. The initial thermal age, which indicates temperature of the lithosphere by conduction only, is varied from 50Ma to 2000Ma. It should be noted that the thermal age is typically different from geological ages. Due to convection in the real Earth, the lithosphere doesn’t cool down significantly after about 600 Ma of geological age. Yet, as we would like to do systematic simulations and obtain the onset of localization versus lithosphere strength and extension strain rate, we still perform simulations with these parameters although they are somewhat unrealistic. Random noise is present in the models because the locations of the tracers are initially randomly perturbed. Tests with prescribed small weak seeds reveal that such weak seed would focus strain localization and result in an earlier occurrence of localization. No additional thermal or rheological heterogeneities are included in the model.

The 2-D simulations are done with the finite element code MILAMIN_VEP (Kaus et al., 2010, Crameri and Kaus 2010). MILAMIN_VEP solves a visco-elasto-plastic problem in a purely Lagrangian manner, and uses remeshing to deal with large deformations. The crust has a Mohr-Coulomb plasticity and the mantle has a low-temperature (Peierls) plasticity (Goetze and Evans, 1979). Shear heating is included. The code has been benchmarked and used in a number of previous studies (e.g. Kaus et al., 2009, Schmeling, et al., 2008, Schmalholz et al., 2009; Crameri & Kaus, 2010). The resolution in this work is set to be 201×201 for the mesh grids. Tests with higher resolution indicate that increasing the resolution yields narrower shear zones but does not alter the overall results significantly. Around 0.2 million randomly distributed markers are used. We find that perturbation introduced by the randomness of markers is sufficient to initiate not only symmetric but also asymmetric localizations.

2.3 1-D semi-analytical model

In order to obtain a better insight in the results of the 2-D simulations, we have also developed a 1-D model, which has exactly the same stratification as the 2-D setup but assumes that the lithosphere is laterally homogeneous and deformed by pure shear extension only. The composition and boundary conditions are laterally homogeneous. The force equilibrium gives:

$$\frac{\partial \sigma_{zz}}{\partial z} + \rho g = 0 \quad (6)$$

The model is first considered visco-elastic:

$$\dot{\varepsilon}_{xx} = \frac{\tau_{xx}}{2\mu} + \frac{1}{2G}\frac{\partial \tau_{xx}}{\partial t}$$

$$\tau_{zz} = -\tau_{xx}, \quad \dot{\varepsilon}_{zz} = -\dot{\varepsilon}_{xx}$$

By discretizing the time term of the equation implicitly, the stress for the new time step at given strain rate is

$$\tau_{xx}^{new} = \frac{2\mu G \Delta t \dot{\varepsilon}_{xx} + \mu \tau_{xx}^{old}}{\mu + G\Delta t}$$

If the stresses are larger than the yielding stresses, plasticity is applied. The plasticity applied in the crust is Mohr-Coulomb yield function (see equation (4)). In the 1-D model, when yielding occurs, the stresses are set to be the yield stresses, i.e.

$$\sigma_1^y = -\sigma_{zz}$$

$$R_M^y = \frac{\sigma_1^y \sin(\phi) + C\cos(\phi)}{1+\sin(\phi)}$$

$$\sigma_3^y = \sigma_1^y - 2R_M^y$$

$$\sigma_{xx} = -\sigma_3^y \quad (7)$$

where R_M^y is the critical radius of Mohr circle of yielding and σ_1^y and σ_3^y are the critical first and third principal stresses of yielding, respectively. σ_{xz} is zero and σ_{zz} is given by equation (6). In the mantle, if the differential stresses are larger than 200 MPa, Peierls plasticity (equation (5)) is applied.

3. 2-D results

Over 300 2-D simulations are performed by systematically varying lithosphere thermal age and extensional strain rate, which results in three end members of deformation modes: no localization, symmetric localization and asymmetric localization (see Figures 2,3,4).

An example of a simulation in which localization does not occur ("*no localization* mode") is shown on Figure 2 (simu592, 10^{-14} s^{-1}, 200Ma). It has a thermal age of 200Ma and an extension strain rate of 10^{-14} s^{-1}. The whole model results in a pure-shear thinning until more than 100% extension. The deformation is homogeneous during extension. The temperature at the Moho, which indicates the potential for thermal localization, is nearly constant which indicates that no localized shear zone is initiated.

A model with the same parameters but with an older thermal age (400Ma) results in *symmetric localization* (simu600, 10^{-14} s^{-1}, 400Ma) (Figure 3). The deformation in this model is relatively homogeneous until ~25% strain. After 50% strain, the lithosphere undergoes necking at the location where a set of symmetric shear zone develop. The temperature at the Moho depth arises locally about 50 degrees up in the shear zone.

If the thermal age of the lithosphere is further increased (1000Ma) with the same overall parameters, *asymmetric localization* occurs (simu591, 10^{-14} s^{-1}, 1000Ma) (Figure 4). Due to the randomness of tracers in our models, the localized shear zone is randomly located. As seen in Figure 4, the shear zone is observable at ~25% strain, and asymmetry is significantly developed at ~30% strain, which is notable in both strain rate and composition fields. Contour plots of temperature indicate that the temperature in the shear zone, which is fully asymmetric, is more than 100 $^{\circ}$C higher in the shear zone compared with the surrounding rocks. The maximum amplitude of localization appears at the upper most mantle.

In our study, localization arises from thermal weakening associated with shear heating. As a result, the temperature in the localized shear zone is larger then that of the surrounding rocks. We can thus distinguish localization from no localization models in an automated manner by using the Moho temperature as a criteria. Here, we consider models to be localized if the Moho temperature is locally >50 $^{\circ}$C higher than the average (see Figures 2,3,4). To distinguish symmetric versus asymmetric localization, however, we use an empirical method based on the 2-D composition and strain rate distribution. Only cases with well-defined narrow shear zones (Figure 4) across the lithosphere are treated as asymmetric localization. Those cases with simple necking of the lithosphere are defined as symmetric localization (Figure 3).

4. Semi-analytical model

In this section we develop a semi-analytical model based on the scaling law derived by Kaus and Podladchikov (2006). Following the work of Crameri and Kaus (2010), we define localization number as

$$I_{loc} = \frac{\dot{\varepsilon}_{bg}\Delta L}{1.4}\sqrt{\frac{\mu_{eff}\gamma}{\kappa\rho c_p}} = \frac{\Delta L}{1.4}\sqrt{\frac{\dot{\varepsilon}_{bg}\tau_{bg}\gamma}{2\kappa\rho c_p}} \qquad (8)$$

, which predicts localization when $I_{loc} > 1$. All parameters are known in the 1-D code described in section 2.2 except the length scale ΔL. The onset of localization is independent on the shear modulus and the initial stress, but is a strong function of the length scale ΔL (Kaus & Podladchikov, 2006). In the work of Kaus and Podladchikov

(2006,) ΔL is simply the radius of initial heterogeneity with a temperature step. However, as we do not introduce any initial thermal or rheological heterogeneity of significant size, the physical meaning of the length scale ΔL in our work is unclear. In the study of Crameri and Kaus (2010) the thickness of plastic layer is used as the characteristic length scale ΔL. Here we take a different approach. Since the mechanism of localization we consider in this work is the coupling of shear heating and temperature-dependent viscosity, here we derive the length scale ΔL based on the additional temperature increase induced by shear heating, compared to a model without shear heating.

First, we consider a simple 1-D heat diffusion model with an initial temperature step ΔT in the center with a width ΔL (see Fig.5a). Temperature diffuses until the maximum temperature becomes slightly smaller than ΔT. As shown in the figure, the initial perturbation width ΔL is approximately equal to the part where temperature is greater than $\Delta T / 2$, which is called "peak width" hereafter. Thus one can recover the initial perturbation width ΔL from a given temperature profile. Similarly, in the current study, the temperature differs from steady state as $T_{diff} = T_{SH} - T_{noSH}$, where T_{SH} is the temperature profile computed in a 1-D model with shear heating, and T_{noSH} that in a model without (H_s=0 in equation 1). Typically a single peak is located in the mantle lithosphere where the stress is largest. Yet in some cases, for example in a warm lithosphere, there will be another smaller peak in the upper crust and this leads to an over-estimating of ΔL. Therefore, we use max(T_{diff})/2+4 as the temperature criteria to compute the length scale ΔL. Tests indicate that the amount of additional 4 degrees is sufficient to overcome this problem while it is negligible once the single peak is dominating.

With the characteristic length scale ΔL being defined and the stress profile (Fig. 6a) being calculated, we can compute I_{loc} as a function of depth for a given setup (Fig. 6b). The maximum of I_{loc} appears in the upper most mantle, consisting with 2-D simulations which show that localization is typically initiated below the Moho (e.g. Figure 4). If the maximum of I_{loc} is greater than 1, localization is expected to occur. As we use a viscoelastic rheology, I_{loc} evolves with time, and a typical evolution of the maximum of I_{loc} for non-localization, symmetric and asymmetric localization as a function of strain is shown in Fig. 6d. Localization is predicted to occur for the setups in Figure 3 and Figure 4, consistent with the numerical results.

Moreover, we can also distinguish different deformation modes of symmetric and asymmetric localization. The evolution of localization number provides insights into the mechanism of localization. In the setup c) (asymmetric localization), I_{loc} first increases rapidly and then decreases after around 15% strain (see Fig. 6d). Although the strain when the localization number gets maximum is somewhat earlier than that of 2-D simulation (see Fig. 4), they are consistent to the first order. The decreasing of localization number may be explained as following. In setup c) with an old thermal age, in which the strength of the lithosphere is quite strong, the rate of thermal energy generated by shear heating is much faster than thermal diffusion and therefore the energy strongly accumulates in a narrow shear band. With the increasing of the maximum of T_{diff}, the width of heterogeneity, as defined by the peak width, becomes narrower (See

Fig. 6c). Thus the localization number reduces when T_{diff} is arising. In this setup, the maximum of T_{diff} exceeds 100^{o}C (Figure 6e), reduces the viscosity by a factor of 10 or more, which was previously demonstrated to be sufficient to result in asymmetric localization (Huismans & Beaumont, 2003). In contrast, in the symmetric localization setup, the localization number increases continuously until the final state. The rate of heat production in this simulation is only slightly larger than the rate of heat conduction. Therefore the width of the peak grows continuously due to the diffusion of T_{diff} at the same time when the energy of shear heating accumulates in the shear zone. I_{loc} increases continuously and gets significantly large when the strain is more than 50%. This is well consistent with 2-D simulations (see Fig. 3) that necking of the lithosphere occurs after 50% of strain. The maximum of T_{diff} in this case is around 50^{o}C, that reduces the viscosity by a factor of around 3. Combining with the fact that the localization number is greater than 1, this predicts a symmetric localized zone, in accordance with 2-D numerical results.

A further probe of viscosity evolution that compares the 1-D model with shear heating (solid lines) with the one without (dash lines) is performed for the setups in which localization develops (see Figure 6f and 6g for setups b) and c), respectively). We show the temporal evolution of both the effective and power law viscosity in the mantle lithosphere, where the effective viscosity includes the effect of low-temperature plasticity. The viscosities in the setups without shear heating remain nearly constant, which indicates that the self-softening effect without shear heating is insufficient to generate localization. In contrast, the viscosities decrease significantly once shear heating is introduced. Whereas the power law viscosity in the setup of *symmetric localization* reduces by a factor of around 3, a factor of >10 for the reduction of power law viscosity occurs in the setup of *asymmetric localization*. Yet the reduction of effective viscosity, in fact the Peierls viscosity here whose rheology does not strongly depend on temperature, is only minor, which is caused by the fact that stresses do not change dramatically in the 1-D model, which is why the mantle lithosphere remains in the Peierls plasticity deformation regime. In 2-D models, however, stress drops very rapidly once the shear zone is initiated (Schmalholz et al., 2009). As a result, the shear-zone deforms in the power law creep regime rather then in the Peierls regime. The power law viscosity reduction of a factor 10 or more is in this case sufficient to induce asymmetric localization (Huismans et al., 2005).

Based on the discussion above, we can thus use the 1-D models to compute a 'phase-diagram' of localization for the standard model (Fig. 7a) and the model with dry olivine mantle (Fig. 7b). Since the thermal age affects the strength of the lithosphere via temperature, which is in reality a key factor of viscosity, we convert thermal ages to temperatures at the depth of 200km on the right side in Figure 7. The boundary between no localization and localization is given by I_{loc}=1. The boundary between symmetric and asymmetric localization is computed by recording the maximum drop of power law viscosity due to shear heating. Asymmetric localization occurs in models in which power law viscosity drops by a factor of 10 or more in the 1-D models. In addition, we have performed 2-D numerical simulations to test the 1-D predictions. The 2-D simulations we have performed cover Earth-like strain rate ranging from 10^{-16} s^{-1} to 10^{-13} s^{-1}. Yet convection is initiated in the asthenosphere in 2-D models with a background strain rate smaller than 5×10^{-15} s^{-1}. In this case, most of the computation is spent on resolving the convection and the simulations become very time consuming. Therefore most of our 2-D simulation results cover relatively fast strain rates. Comparisons of such phase-diagrams and 2-D results are plotted in Figure 7 for both the standard setup and the one with dry olivine mantle. The different mechanical modes of deformation predicted by the semi-analytical model are highlighted as shaded areas. Insets of 2-D simulations for the setups discussed above illustrate different modes of deformation (Fig. 7). There is a good agreement between 1-D and 2-D results, which thus demonstrates that the semi-analytical model is capable of predicting the onset of symmetric/asymmetric localization.

5. Applications

Stability of cratons

A number of studies addressed the longevity of cratons to the chemical buoyancy due to high degrees of melt-depletion and the high viscosity imparted by the low temperatures (Jordan, 1975,1978; Pollack, 1986; Doin et al., 1997; Shapiro et al., 1999; Sengor, 1999). However, geodynamic calculations suggested that they are relatively insufficient to prevent the cratonic root from being recycled during convection over billions of years (Lenardic et al., 2000, 2003; Sleep, 2003; O'Neill et al., 2008). A recent analysis showed that cratons are more likely to be generated if the Rayleigh number of the mantle is larger, such as was the case in the Archean (Cooper and Conrad, 2010). The decrease of mantle Rayleigh-number with time increases basal tractions, which makes it more likely for the craton to be destroyed. Yet, as soon as a craton is surrounded by weak zones, the stresses associated with mantle convection are buffered and the craton is prevented from being further deformed (Lenardic et al., 2000,2003). Such weak zones could result from either symmetric or asymmetric localization of the lithosphere under extension, and additionally contribute to the longevity of cratons.

Our semi-analytical model predicts a wide range of parameter space for localization for both the standard model and the model with dry olivine mantle. On one hand, at a certain extension strain rate, a cold thermal state (old thermal age) tends to develop localization, while the lithosphere under a hot thermal state (young thermal age) is more likely to deform without localization. The conditions for localization predicted in our study are in good agreements with the initial thermal condition that forms narrow rifts (Buck, 1991). Buck (1991) pointed out that none of narrow rifts were formed in a hot lithosphere (with a heat flow higher than 60-70mW m^{-2}). Therefore a sufficient cold thermal state is required to keep cratons stable. On the other hand, with a certain thermal age, faster deformation is favored to initiate localization. For cratonic thermal ages (>400Ma), a major part of Earth-like extension strain rate locates in the region of localization, with dry lithosphere developing localization easier than wet lithosphere. It implies that most cratons can form narrow rifts and keep stable. In other words, it is more likely that cratons may deform uniformly without localization under very slow extension or in a water-rich condition.

Water in the Mantle Lithosphere

The strength of olivine is strongly dependent on the content of water (Chopra & Paterson, 1984; Karato, 1986; Mackwell et al., 1985; Hirth & Kohlstedt, 1996; Kohlstedt, 2006). The water content in the upper mantle may vary regionally (Huang et al., 2005; Katayama et al., 2005; Ichiki et al., 2006; Peslier, et al., 2010). A recent study by Karato

(2011) has suggested high water content (up to 1 wt%) in the mantle transition zone, with eastern China significantly higher than other continental regions. Some authors (e.g. Zhu & Zheng, 2009) suggested that the destruction of NCC may be related to water content in the mantle. The NCC is one of the most striking examples for the destruction of cratons, which was proposed to have formed in the Paleoproterozoic age by the amalgamation of two Archean blocks, the western (or “Ordos”) and eastern blocks, along the Trans-North China orogen (or “Central Block”) (e.g. Zhao et al.,2001). Later in the late Mesozoic and Cenozoic, the eastern part underwent from having a thick (~200km) lithosphere to its current much thinner lithosphere (60-80 km) (Griffin et al, 1998; Chen et al., 2006a, 2008; Zheng et al., 2008,2009; Zhao et al., 2009). The western part however remains stable, with a lithosphere thicker than 200 km (Chen et al., 2009; Zhao et al., 2009; Chen, 2010). A narrow rift (Shaanxi-Shanxi Rift on the order of 100 km wide) in the Central Block seperates the NCC into the stable western block and the destructed eastern block (Zhao & Xue, 2010). The eastern NCC is believed to have been affected by an extensional stress field, as evidenced by a series of half-graben basins as well as seismic anisotropy patterns (Ren et al., 2002; Zhao & Zheng, 2005; Zhao et al., 2007,2008). It has formed a basin (Bohai Bay Basin) with a maximum width of about 450km (Chen et al., 2006b; Zhao & Xue, 2010). Receiver function studies (Chen et al., 2006b; Zheng et al., 2007,2008,2009) showed a thinned (~30 km) crust with small thickness variations in the eastern NCC compared to a thicker (~40 km) crust in the western NCC. It thus suggests that the eastern NCC has deformed in a “wide rifting” mode. A seismic tomography study beneath the northeast Asia shows a stagnated slab in the mantle transition zone, whose front end is located below the boundary of the eastern and western NCC (Zhao & Ohtani, 2009; Huang et al. 2006). It is thus possible that the lithosphere of the eastern NCC is water-rich due to the dehydration of the subducted oceanic slab compared to the western NCC.

Here we apply our semi-analytical model to both the eastern and western NCC. Since the western NCC is stable, it is reasonable to take its present-day stratification as the pre-extension model for the eastern NCC. Our eastern/western NCC model is defined having a 200km lithosphere, including a 25km upper crust and a 15km lower crust. The rheologies for the upper crust and lower crust are the same as that in the standard model. The rheologies for the mantle, however, are different. "Dry olivine" is applied in the western NCC model while "wet olivine" is used in the eastern NCC model. The results for the occurrence of localization show that the thermal age required for localization in the western NCC model at a certain background strain rate (say ~10^{-15} s^{-1}) is generally younger than that in the eastern NCC model (Fig. 8a). This implies the western NCC is easier to develop localization and form narrow rifts, which keeps the western NCC stable. In contrast, the eastern NCC tends to deform without localization. The shaded area in Figure 8a indicates the conditions under which the western NCC is stable and the eastern NCC is destructed. For the NCC prior to extension, in which the thermal age is assumed to be 500Ma, the temperature is about 1300^{o}C at the base of the 200-km thick lithosphere. According to the prediction, our model constraints the maximum extension strain rate of NCC to be 1×10^{-15} s^{-1}. Considering the thinning of crustal thickness from 40km to 30km in the eastern NCC, such a strain rate predicts a minimum extension period of ~10Ma. This coincides in the first order with the duration of large-scale gold mineralization (Yang et al., 2003) and magmatic activity (Wu et al., 2005) in this region.

As the next step, we combine our semi-analytical model with a rheology of wet olivine which is a function of water concentration that is introduced by Li et al. (2008). We take all parameters from Li's study except ignoring activation volume due to the lack of pressure dependency in our model. The flow law of olivine is given as (Mei & Kohlstedt, 2000)

$$\dot{\varepsilon} = A_{cre}\tau^{n_1} f_{H_2O}^{r} \exp(-\frac{Q_{cre}}{RT})$$

with $A_{cre} = 1600\text{MPa}^{-(n_1+r)}\text{s}^{-1}$, $n_1 = 3.5$, $r = 1.2$, $Q_{cre} = 530\text{kJ mol}^{-1}$; $\dot{\varepsilon}$ and τ are strain rate and shear stress, respectively.

$$f_{H_2O} = \exp(c_0 + c_1 \ln C_{OH} + c_2 \ln^2 C_{OH} + c_3 \ln^3 C_{OH})$$

is water fugacity, with $c_0 = -7.9859$, $c_1 = 4.3559$, $c_2 = -0.5742$, $c_3 = 0.0337$, and f_{H_2O} in MPa and C_{OH} is water concentration in H/10^{6}Si.

By fixing thermal age at 500Ma for cratonic condition, and varying extension strain rate and water concentration, our prediction suggests that the critical minimum water concentration required to let the Eastern NCC deform without localization depends on the extension strain rate (Figure 8b). For small strain rates, less water is required for the Eastern NCC to keep remaining in the "no localization" phase. Once the extension strain rate is determined, the critical amount of water can then be obtained. Given the maximum extension strain rate for the Eastern NCC, for example, at 10^{-15} s^{-1}, at most ~3000 H/10^{6}Si of water is sufficient to reduce the strength of the lithosphere and make it deform in the manner of wide-rift. This is comparable with water content in the mantle transition zone or subduction zones suggested by other studies (e.g. Dixon et al. 2004; Karato 2011).

However, whereas the crust in the eastern NCC thins from ~40km to ~30km, the lithosphere has much larger thinning from ~200km to ~100km, due to differential thinning (e.g. McKenzie, 1978; Steckler, 1985; White & McKenzie, 1988), which is not well predicted in our model. Some other mechanisms might thus also partly contribute to the thinning of the lithosphere. Hydration alone, for example, could weaken the lithosphere and initiate the thinning of the mantle lithosphere (Li et al., 2008). It has been suggested (Komiya & Maruyama 2007; Kusky et al., 2007) that the dual subduction of the Pacific and Indo-Australian plates may double the amount of water transported into the mantle transition zone under the marginal basins of the Western Pacific and under the North China Craton. Therefore, the mantle transition zone might be a reservoir of water during plate tectonics and raises a possibility to hydrate the lithosphere of the eastern NCC before extension.

Peierls strength

Only a few experiments on low temperature plasticity (Peierls plasticity) have been carried out over the past decades (Goetze, 1978; Evans & Goetze, 1979; Raterron et al., 2004; Katayama & Karato, 2008; Mei et al, 2010), and as a consequence, the flow laws are not well constrained. In order to better understand the effect of uncertainties in experimental parameters on the initiation of shear localization we compare results of a newly derived Peierls plasticity flow law (Mei et al., 2010) with the one used in this study (Goetze and Evans, 1979) (Fig. 9), which can be evaluated in a rapid manner using our 1-D models. The flow law of the newly derived Peierls plasticity by Mei et al. (2010) is described as

$$\dot{\varepsilon} = A_P \sigma^2 \exp(-\frac{E_k(0)}{RT}(1-\sqrt{\frac{\sigma}{\sigma_P}})) \quad (9)$$

with A_P =1.4×10^{-7} s^{-1} MPa^{-2}, $E_k(0)$ =320 km mol^{-1} and σ_P =5.9 GPa. A plot of "Christmas Tree" indicates that the Peierls plasticity by Goetze and Evans (1979) has higher strength in the mantle (Fig. 9a). The prediction results (Fig. 9b) illustrate that the general trends remain the same but that Peierls plasticity affects both symmetric and asymmetric localization in parameter space with old thermal ages (>400Ma), in which the temperature of the lithosphere is low enough to meet the condition for "low-temperature" plasticity. Both symmetric and asymmetric localization is easier to initiate for the model with Peierls plasticity by Goetze and Evans (1979). In particular, the slower of the extension strain rate, the more important of the influence. Therefore simulations with a higher Peierls plasticity are more likely to develop localized zones, and suggest increasing possibility of stabilizing cratons.

6. Conclusions

We perform a systematic study on the conditions of strain localization in a thick lithosphere under extension, in which localization is caused by shear-heating related thermal weakening. In systematic 2-D models, we observe three end members of deformation of the lithosphere under extension, i.e. no localization, symmetric localization and asymmetric localization. A semi-analytical method is developed that gives insights in the underlying physics and helps to constrain the conditions for each of those end members. Sharp boundaries exist between different modes of deformation. We conclude that

(1) A cold thermal state tends to develop lithospheric localization in comparison with a hot thermal state.

(2) Faster deformation and colder thermal state are required to form lithospheric asymmetric localization in comparison with symmetric localization in our standard setup.

(3) Mantle lithosphere with dry olivine rheology promotes the occurrence of localization.

(4) Model Peierls's plasticity that results in larger differential stresses (Goetze and Evans, 1979) predicts localization to occur easier.

Applications to the destruction of cratons and continental break-up are discussed. As localization forms narrow rifts and protects cartons from being destructed, higher strength of the lithosphere, e.g. stronger rheology and colder thermal state, as well as faster deformation increases the likelihood that a localized lithospheric rift occurs, which shields the remaining pieces of the craton from subsequent deformation. Lithospheres with a weaker rheology instead deform in a homogeneous manner similar to the formation of wide rifts.

Acknowledgements

We thank Tianyu Zheng, Ling Chen, Yumei He, and Marcel Thielmann for discussions, and reviewers Adrian Lenardic and Craig O'Neil for helpful suggestions that improved the paper.This research was financially supported by the NSFC Grant 90814002 and 40974030.

References

Afonso, J.C., G. Ranalli, 2004. Crustal and mantle strengths in continental lithosphere: is the jelly sandwich model obsolete?, Tectonophysics 394, 221-232.

Armitage, J.J., P.A. Allen, 2010. Cratonic basins and the long-term subsidence history of continental interiors, Journal of the Geological Society, 167, 61-70.

Artemieva, I.M., 2009. The continental lithosphere: Reconciling thermal, seismic, and petrologic data. Lithos 109, 23-46.

Ashby, M.F., C.G. Sammis, 1990. The Damage Mechanics of Brittle Solids in Compression. Pure Appl. Geophys. 133, 489-521.

Bercovici, D., 1996. Plate generation in a simple model of lithosphere-mantle flow with dynamic self-lubrication. Earth Planet. Sci. Lett. 144, 41-51.

Bercovici, D., Y. Ricard, G. Schubert, 2001a. A two-phase model for compaction and damage 1. General Theory. J. Geophys. Res. 106, 8887-8906.

Bercovici, D., Y. Ricard, G. Schubert, 2001b. A two-phase model for compaction and damage 3. Applications to shear localization and plate boundary formation. J. Geophys. Res. 106, 8925-8939.

Bercovici, D., S. Karato, 2003. Theoretical analysis of shear localization in the lithosphere. Plastic Deformation of Minerals and Rocks 51, 387-420.

Braeck, S. and Y.Y. Podladchikov, 2007. Spontaneous thermal runaway as an ultimate failure mechanism of materials. Phys. Rev. Lett. 98, Doi 10.1103/Physrevlett.98.095504.

Braun, J., J. Chery, A. Poliakov, D. Mainprice, A. Vauchez, A. Tommasi, M. Daignieres, 1999. A simple parameterization of strain localization in the ductile regime due to grain size reduction: A case study for olivine. J. Geophys. Res. 104, 25167-25181.

Buck, W.R., 1991. Modes of continental lithospheric extension. J. Geophys. Res. 96, 20161-20178.

Buck, W.R., L.L. Lavier, A.N.B. Poliakov, 1999. How to make a rift wide. Philosophical Transactions of the Royal Society of London Series a-Mathematical Physical and Engineering Sciences 357, 671-690.

Burg, J. P. and S. M. Schmalholz, 2008. Viscous heating allows thrusting to overcome crustal-scale buckling: Numerical investigation with application to the Himalayan syntaxes. Earth Planet. Sci. Lett. 274, 189-203.

Burov, E., F. Houdry, M. Diament, J. Deverchere, 1994. A broken plate beneath the North Baikal Rift-Zone revealed by gravity modeling. Geophys. Res. Lett. 21, 129-132.

Carlson, R.W., A.J. Irving, D.J. Schulze, C. Hearn, 2004. Timing of Precambrian melt depletion and Phanerozoic refertilization events in the lithospheric mantle of the Wyoming Craton and adjacent Central Plains Orogen. Lithos 77, 453-472.

Chen, L., 2010. Concordant structural variations from the surface to the base of the upper mantle in the North China Craton and its tectonic implications. Lithos doi:10.1016/j.lithos.2009.12.007.

Chen, L., T.Y. Zheng, W.W. Xu, 2006a. A thinned lithospheric image of the Tanlu Fault Zone, eastern China: Constructed from wave equation receiver migration. J. Geophys. Res. 111, Doi 10.1029/2005jb003974.

Chen, L., T.Y. Zheng, W.W. Xu, 2006b. Receiver function migration image of the deep structure in the Bohai Bay Basin, eastern China. Geophys. Res. Lett. 33, Doi 10.1029/2006gl027593.

Chen, L., W. Tao, L. Zhao, T.Y. Zheng, 2008. Distinct lateral variation of lithospheric thickness in the northeastern North China Craton. Earth Planet. Sci. Lett. 267, 56-68.

Chen, L., C. Cheng, Z.G. Wei, 2009. Seismic evidence for significant lateral variations in lithospheric thickness beneath the central and western North China Craton. Earth Planet. Sci. Lett. 286, 171-183.

Chen, W.P. and P. Molnar, 1983. Focal Depths of Intracontinental and Intraplate Earthquakes and Their Implications for the Thermal and Mechanical-Properties of the Lithosphere. Journal of Geophysical Research, 88, 4183-4214.

Chopra, P. N., M. S. Paterson, 1984, The role of water in the deformation of dunite, J. Geophys. Res.,89, 7861-7876.

Cooper, C.M., C.P. Conrad, 2009. Does the mantle control the maximum thickness of cratons? Lithosphere 1, 67-72.

Crameri, F. and B.J.P. Kaus, 2010. Parameters that control lithospheric-scale thermal localization on terrestrial planets. Geophys. Res. Lett. 37, Doi 10.1029/2010gl042921.

Dabrowski, M., M. Krotkiewski, and D.W. Schmid, 2008. MILAMIN: MATLAB-based finite element method solver for large problems. Geochem. Geophys. Geosyst. 9, doi:10.1029/2007GC001719.

Deverchere, J., C. Petit, N. Gileva, N. Radziminovitch, V. Melnikova, V. San’kov, 2001. Depth distribution of earthquakes in the Baikal rift system and its implications for the rheology of the lithosphere. Geophys. J. Int. 146, 714-730.

Deverchere, J., F. Houdry, M. Diament, N.V. Solonenko, A.V. Solonenko, 1991. Evidence for a Seismogenic Upper Mantle and Lower Crust in the Baikal Rift. Geophy. Res. Lett. 18, 1099-1102.

Dixon, J.E., T.H. Dixon, D.R. Bell, R. Malservisi, 2004. Lateral variation in upper mantle viscosity: role of water. Earth Planet. Sci. Lett. 222, 451-467.

Doglioni, C., E. Carminati, E. Bonatti, 2003. Rift asymmetry and continental uplift. Tectonics 22, Doi 10.1029/2002tc001459.

Doin, M.-P., L. Fleitout, U. Christensen, 1997. Mantle convection and stability of depleted and undepleted continental lithosphere. J. Geophys. Res. 102, 2771-2787.

Eggler, D.H., J.K. Meen, F. Welt, F.O. Dudas, K.P. Furlong, M.E. Mccallum, R.W. Carlson, 1988. Tectonomagmatism of the Wyoming Province. Colorado School of Mines Quarterly 83, 25-40.

Emmerson, B., J. Jackson, D. McKenzie, K. Priestley, 2006. Seismicity, structure and rheology of the lithosphere in the Lake Baikal region. Geophys. J. Int. 167, 1233-1272.

England, P., 1983. Constraints on extension of continental lithosphere. J. Geophys. Res. 88, 1145-1152.

Evans, B., C. Goetze, 1979. Temperature-variation of hardness of olivine and its implication for polycrystalline yield stress. J. Geophy. Res. 84, 5505-5524.

Fan, W., M. Menzies, 1992. Destruction of aged lower lithosphere and accretion of asthenosphere mantle beneath eastern China. Geotectonica et Metallogenia 16, 171-180.

Gao., S., P. Davis, H. Liu, P. Slack, Y. Zorin, N. Logatchev, M. Kogan, P. Burkholder, R. Meyer, 1994. Asymmetric upwarp of the asthenosphere beneath the Baikal Rift-Zone, Siberia. J. Geophys. Res. 99, 15319-15330.

Goetze, C., 1978. Stress and Temperature in Bending Lithosphere as Constrained by Experimental Rock Mechanics. Transactions-American Geophysical Union 59, 372-372.

Goetze, C., B. Evans, 1979. Stress and temperature in the bending lithosphere as constrained by experimental rock mechanics. Geophys. J. R. Astron. Soc. 59, 463-478.

Griffin, W., Z. Andi, S. O'Reilly, C. Ryan, 1998. Phanerozoic evolution of the lithosphere beneath the Sino-Korean Craton. Mantle Dynamics and Plate Interactions in East Asia 27, 107-126.

Gueydan, F., C. Morencey, J. Brun, 2008. Continental rifting as a function of lithosphere mantle strength. Tectonophysics 460, 83-93.

Hirth, G., D.L. Kohlstedt, 1996. Water in the oceanic upper mantle: Implications for rheology, melt extraction and the evolution of the lithosphere. Earth Planet. Sci. Lett. 144, 93-108.

Huang, J.L., and D. Zhao, 2006. High-resolution mantle tomography of China and surrounding regions. J. Geophys. Res. 111, B09305, doi:10.1029/2005JB004066.

Huang, X.G., Y.S. Xu, S.I. Karato, 2005. Water content in the transition zone from electrical conductivity of wadsleyite and ringwoodite. Nature 434, 746-749.

Huismans, R.S., C. Beaumont, 2002. Asymmetric lithospheric extension: The role of frictional strain softening inferred from numerical experiments. Geology 30, 211-214.

Huismans, R.S., C. Beaumont, 2003. Symmetric and asymmetric lithospheric extension: Relative effects of frictional-plastic and viscous strain softening. J. Geophys. Res. 108, Doi 10.1029/2002jb002026

Huismans, R.S., S.J.H. Buiter, C. Beaumont, 2005. Effect of plastic-viscous layering and strain softening on mode selection during lithospheric extension. J. Geophys. Res. 110, Doi 10.1029/2004jb003114.

Ichiki, M., K. Baba, M. Obayashi, H. Utada, 2006. Water content and geotherm in the upper mantle above the stagnant slab: Interpretation of electrical conductivity and seismic P-wave velocity models. Phys. Earth Planet. Int. 155, 1-15.

Jackson, J.A., 2002a. Faulting, flow, and the strength of the continental lithosphere. International Geology Review 44, 39-61.

Jackson, J.A., 2002b. Strength of the continental lithosphere: time to abandon the jelly sandwich? GSA Today 12, 4-10.

Jin, D.H., S.I. Karato, M. Obata, 1998. Mechanisms of shear localization in the continental lithosphere: Inference from deformation microstructures of peridotites from the Ivrea zone, northwestern Italy. Journal of Structural Geology 20, 195-209.

Jordan, T.H., 1975. The continental tectosphere. Rev. Geophys. 13, 1-12.

Jordan, T.H., 1978. Composition and development of the continental tectosphere. Nature 274, 544-548.

Kameyama, M., D.A. Yuen, H. Fujimoto, 1997. The interaction of viscous heating with grain-size dependent rheology in the formation of localized slip zones. Geophys. Res. Lett. 24, 2523-2526.

Kameyama, M., D.A. Yuen, S.I. Karato, 1999. Thermal-mechanical effects of low-temperature plasticity (the Peierls mechanism) on the deformation of a viscoelastic shear zone. Earth Planet. Sci. Lett. 168, 159-172.

Kaus, B.J.P., 2009. Factors that control the angle of shear bands in geodynamic numerical models of brittle deformation. Tectonophysics 484, 36-47.

Kaus, B.J.P., H. Muhlhaus, D.A. May, 2010. A stabilization algorithm for geodynamic numerical simulations with a free surface. Phys. Earth Planet. Int. 181, 12-20.

Kaus B.J.P., Y. Liu, T.W. Becker, D.A. Yuen, Y. Shi, 2009. Lithospheric stress-states predicted from long-term tectonic models: Influence of rheology and possible application to Taiwan. J. Asian Earth Sci. 36, 119-134.

Kaus, B.J.P., Y.Y. Podladchikov, 2006. Initiation of localized shear zones in viscoelastoplastic rocks. J. Geophys. Res. 111, B04412, doi:10.1029/2005JB003652.

Karato, S.I., M.S. Paterson, J.D. Fitz Gerald, 1986. Rheology of synthetic olivine aggregates - Influence of grain-size and water. J. Geophys. Res. 91, 8151-8176.

Karato, S.-I., 2011. Water distribution across the mantle transition zone and its implications for global material circulation. Earth Planet. Sci. Lett. 301, 413-423.

Katayama, I. and S.I. Karato, 2008. Effects of water and iron content on the rheological contrast between garnet and olivine. Phys. Earth Planet. Int. 166, 57-66.

Katayama, I., S.I. Karato, M. Brandon, 2005. Evidence of high water content in the deep upper mantle inferred from deformation microstructures. Geology 33, 613-616.

Kohlstedt, D.L., 2006. The role of water in high-temperature rock deformation. Water in Nominally Anhydrous Minerals 62, 377-396.

Komiya, T. and S. Maruyama, 2007. A very hydrous mantle under the western Pacific region: Implications for formation of marginal basins and style of Archean plate tectonics. Gondwana Research 11, 132-147.

Kusky, T.M., B.F. Windley, M.G. Zhai, 2007. Lithospheric thinning in eastern Asia; constraints, evolution, and tests of models. Mesozoic Sub-Continental Lithospheric Thinning under Eastern Asia 280, 331-343.

Landuyt, W., D. Bercovici, 2009. Formation and structure of lithospheric shear zones with damage. Phy. Earth Planet. Int. 175, 115-126.

Lenardic, A., L.N. Moresi, H. Muhlhaus, 2000. The role of mobile belts for the longevity of deep cratonic lithosphere: The crumple zone model. Geophys. Res. Lett. 27, 1235-1238.

Lenardic, A., L.N. Moresi, H. Muhlhaus, 2003. Longevity and stability of cratonic lithosphere: Insights from numerical simulations of coupled mantle convection and continental tectonics. J. Geophys. Res. 108, Doi 10.1029/2002jb001859.

Li, Z.-X. A., C.-T. A. Lee, A.H. Peslier, A. Lenardic, S.J. Mackwell, 2008. Water contents in mantle xenoliths from the Colorado Plateau and vicinity: Implications for the mantle rheology and hydration-induced thinning of continental lithosphere. J. Geophys. Res. 113, B09210, doi:10.1029/2007JB005540.

Mackwell, S.J., D.L. Kohlstedt, M.S. Paterson, 1985. The role of water in the deformation of olivine single-crystals. J. Geophys. Res. 90, 1319-1333.

Maggi, A, J.A. Jackson, D. McKenzie, K. Priestley, 2000a. Earthquake focal depths, effective elastic thickness, and the strength of the continental lithosphere. Geology 28, 495-498.

Maggi, A, J.A. Jackson, K. Priestley, C. Baker, 2000b. A re-assessment of focal depth distributions in southern Iran, the Tien Shan and northern India: do earthquakes really occur in the continental mantle? Geophys. J. Int. 143, 629-661.

McKenzie, D., 1978. Some remarks on development of sedimentary basins. Earth Planet. Sci. Lett. 40, 25-32.

Mei, S., A.M. Suzuki, D.L. Kohlstedt, N.A. Dixon, W.B. Durham, 2010. Experimental constraints on the strength of the lithospheric mantle. J. Geophys. Res. 115, 10.1029/2009JB006873

Mei, S., D.L. Kohlstedt, 2000. Influence of water on plastic deformation of olivine aggregates 2. Dislocation creep regime. J. Geophys. Res. 105, 21471-21481.

Meissner, R., W. Mooney, 1998. Weakness of the lower continental crust: a condition for delamination, uplift, and escape. Tectonophysics 296, 47-60.

Menzies, M. A., W. Fan, M. Zhang, 1993. Palaeozoic and Cenozoic lithoprobes and the loss of >120 km of Archaean lithosphere, Sino-Korean craton, China. Geological Society, London, Special Publications 76, 71-81.

Montesi, L.G.J., M.T. Zuber, 2002. A unfied description of localization for application to large-scale tectonics. J. Geophy. Res.-Solid Earth 107, 1-17.

Mooney, W.D., G. Laske, T.G. Masters, 1998. CRUST 5.1: A global crustal model at 5 degrees x 5 degrees. J. Geophys. Res. 103, 727-747.

Ogawa, M., 1987. Shear Instability in a Viscoelastic Material as the Cause of Deep-Focus Earthquakes. J. Geophys. Res.-Solid Earth and Planets 92, 13801-13810.

O'Neill, C.J., A. Lenardic, W.L. Griffin, S.Y. O'Reilly, 2008. Dynamics of cratons in an evolving mantle. Lithos 102, 12-24.

Peslier, A.H., A.B. Woodland, D.R. Bell, M. Lazarov, 2010. Olivine water contents in the continental lithosphere and the longevity of cratons. Nature 467, 78-U108, doi: 10.1038/nature09317

Petit, C., E. Burov, J. Deverchere, 1997. On the structure and mechanical behaviour of the extending lithosphere in the Baikal rift from gravity modelling. Earth Planet. Sci. Lett. 149, 29-42.

Petit, C., J. Deverchere, 2006. Structure and evolution of the Baikal rift: A synthesis. Geochem. Geophys. Geosyst. 7, Doi 10.1029/2006gc001265.

Petit, C., I. Koulakov, J., Deverchere, 1998. Velocity structure around the Baikal rift zone from teleseismic and local earthquakes traveltimes and geodynamic implications. Tectonophysics 296, 125-144.

Pollack, H.N., 1986. Cratonization and thermal evolution of the mantle. Earth Planet. Sci. Lett. 80, 175-182.

Precigout, J., F. Gueydan, 2009. Mantle weakening and strain localization: Implications for the long-term strength of the continental lithosphere. Geology 37, 147-150.

Priestley, K., J. Jackson, D. McKenzie, 2008. Lithospheric structure and deep earthquakes beneath India, the Himalaya and southern Tibet. Goephys. J. Int. 172, 345-362.

Raterron, P., Y.J. Wu, D.J. Weidner, J.H. Chen, 2004. Low-temperature olivine rheology at high pressure. Phys. Earth Planet. Int. 145, 149-159.

Radziminovich, N.A., 2010. Focal depths of earthquakes in the Baikal region: A review. Izvestiya - Phys. Solid Earth 46, 216-229.

Regenauer-Lieb, K., 1999. Dilatant plasticity applied 10 Alpine collision: ductile void growth in the intraplate area beneath the Eifel volcanic field. J. Geodynamics 27, 1-21.

Regenauer-Lieb, K., D.A. Yuen, J. Branlund, 2001. The initiation of subduction: Criticality by addition of water? Science 294, 578-580.

Regenauer-Lieb, K., D.A. Yuen, 2004. Positive feedback of interacting ductile faults from coupling of equation of state, rheology and thermal-mechanics. Phys. Earth Planet. Int. 142, 113-135.

Ren, J.Y., K. Tamaki, S.T. Li, J.X. Zhang, 2002. Late Mesozoic and Cenozoic rifting and its dynamic setting in Eastern China and adjacent areas. Tectonophysics 344, 175-205.

San'kov, V., J. Deverchere, Y. Gaudemer, F. Houdry, A. Filippov, 2000. Geometry and rate of faulting in the North Baikal Rift, Siberia. Tectonics 19, 707-722.

Schmalholz, S.M., B.J.P. Kaus, J.P. Burg, 2009. Stress-strength relationship in the lithosphere during continental collision. Geology 37, 775-778.

Schmeling, H. , A.Y. Babeyko, A. Enns, C. Faccenna, F. Funiciello, T. Gerya, G.J. Golabek, S. Grigull, B.J.P. Kaus, G. Morra, S.M., Schmalholz, J. van Hunen, 2008. A benchmark comparison of spontaneous subduction models - towards a free surface. Phys. Earth Planet.Int. 171, 198-223.

Schubert, G. and D.L. Turcotte,1972. One-Dimensional Model of Shallow-Mantle Convection. J. Geophys. Res. 77, 945-951.

Sengor, A.M.C., 1999. Continental interiors and cratons: any relation? Tectonophysics 305, 1-42.

Shapiro, S.S., B.H. Hager, T.H. Jordan, 1999. Stability and dynamics of the continental tectosphere. Lithos 48, 1-4.

Sleep, N.H., 2003. Survival of Archean cratonal lithosphere. J. Geophys. Res. 108, doi: 10.1029/2001JB000169.

Steckler, M.S., 1985. Uplift and extension at the Gulf of Suez - Indications of induced mantle convection. Nature 317, 135-139.

Stern, R.J., 1994. Arc Assembly and Continental Collision in the Neoproterozoic East-African Orogen - Implications for the Consolidation of Gondwanaland. Annu. Rev. Earth Planet. Sci. 22, 319-351.

Tommasi, A., M. Knoll, A. Vauchez, J. Signorelli, C. Thoraval, R. Loge, 2009. Structural reactivation in plate tectonics controlled by olivine crystal anisotropy. Nature Geoscience 2, 422-426.

Wernicke, B., 1981. Low-angle normal faults in the Basin and Range Province: nappe tectonics in an extending orogen. Nature 291, 645-648.

Westaway, R., 1995. Crustal Volume Balance during the India-Eurasia Collision and Altitude of the Tibetan Plateau - a Working Hypothesis. J. Geophys. Res.-Solid Earth 100, 15173-15192.

White, N., D. Mckenzie, 1988. Formation of the Steers Head Geometry of Sedimentary Basins by Differential Stretching of the Crust and Mantle. Geology 16, 250-253.

Wu, F.Y., J.Q. Lin, S.A. Wilde, X.O. Zhang, J.H. Yang, 2005. Nature and significance of the Early Cretaceous giant igneous event in eastern China. Earth Planet. Sci. Lett. 233, 103-119.

Yang, J.H., F.Y. Wu, S.A. Wilde, 2003. A review of geodynamic setting of large-scale Late Mesozoic gold mineralization in the North China Craton: an association with lithospheric thinning. Ore Geology Reviews 23, 125-152.

Zandt, G., S.C. Myers, T.C. Wallace, 1995. Crust and Mantle Structure across the Basin and Range Colorado Plateau Boundary at 37-Degrees-N Latitude and Implications for Cenozoic Extensional Mechanism. J. Geophys. Res.-Solid Earth 100, 10529-10548.

Zhao, G.C., S.A. Wilde, P.A. Cawood, M. Sun, 2001. Archean bolocks and their boundaries in the North China Craton: lithological, geochemical, structural and P-T path constraints and tectonic evolution. Precambiran Res. 107, 45-73.

Zhao, D., E. Ohtani, 2009. Deep slab subduction and dehydration and their deodynamic consequences: Evidence from seismology and mineral physics. Gondwana Res. 16, 401-413.

Zhao, L., M. Xue, 2010. Mantle flow pattern and geodynamic cause of the North China Craton reactivation: Evidence from seismic anisotropy. Geochem. Geophys. Geosyst. 11, Doi 10.1029/2010gc003068.

Zhao, L., R.M. Allen, T. Zheng, S.H. Hung, 2009, Reactivation of an Archean craton: Constraints from P- and S-wave tomography in North China. Geophys. Res. Lett. 36, doi:10.1029/2009GL039781.

Zhao, L., T.Y. Zheng, 2005. Using shear wave splitting measurements to investigate the upper mantle anisotropy beneath the North China Craton: Distinct variation from east to west. Geophys. Res. Lett. 32, Doi 10.1029/2005gl022585.

Zhao, L., T.Y. Zheng, G. Lu, 2008. Insight into craton evolution: Constraints from shear wave splitting in the North China Craton. Phys. Earth Planet. Int. 168, 153-162.

Zhao, L., T.Y. Zheng, L. Chen, Q.S. Tang, 2007. Shear wave splitting in eastern and central China: Implications for upper mantle deformation beneath continental margin. Phys. Earth Planet. Int. 162, 73-84.

Zhao, W.L., W.J. Morgan, 1985. Uplift of Tibetan Plateau. Tectonics 4, 359-369.

Zhao, W.L., W.J. Morgan, 1987. Injection of Indian Crust into Tibetan Lower Crust - a Two-Dimensional Finite-Element Model Study. Tectonics 6, 489-504.

Zheng, T.Y., L. Chen, L. Zhao, R.X. Zhu, 2007. Crustal structure across the Yanshan belt at the northern margin of the North China Craton. Phys. Earth Planet. Int. 161, 36-49.

Zheng, T.Y., L. Zhao, R.X. Zhu, 2009. New evidence from seismic imaging for subduction during assembly of the North China craton. Geology 37, 395-398.

Zheng, T.Y., L. Zhao, W.W. Xu, R.X. Zhu, 2008. Insight into modification of North China Craton from seismological study in the Shandong Province. Geophys. Res. Lett. 35, Doi 10.1029/2008gl035661.

Zhu, R.X., T.Y. Zheng, 2009. Destruction geodynamics of the North China craton and its Paleoproterozoic plate tectonics. Chinese Sci. Bull. 54, 3354-3366.

TABLE 1: APPLIED ROCK-PHYSICAL AND RHEOLOGICAL PARAMETERS

	Upper crust (Wet quartzite)	Lower crust, weak (Diabase)	Lower crust, strong (Columbia diabase)	Mantle, wet (Wet olivine)	Mantle, dry (Dry olivine)
Elastic Shear Module(Pa)	1×10^{10}	1×10^{10}	1×10^{10}	1×10^{10}	1×10^{10}
Prefactor(s^{-1} Pa^{-n})	5.07×10^{-18}	3.2×10^{-20}	1.2×10^{-26}	4.89×10^{-15}	4.85×10^{-17}
Activation Energy($J\cdot mol^{-1}$)	154×10^{3}	276×10^{3}	485×10^{3}	515×10^{3}	535×10^{3}
Power law exponent	2.3	3.0	4.7	3.5	3.5
Density($kg\cdot m^{-3}$)	2800	2900	2900	3300	3300
Cohesion(Pa)	1×10^{7}	1×10^{7}	1×10^{7}	1×10^{7}	1×10^{7}
Friction angle(°)	30	30	30	30	30
Thermal Conductivity($W\cdot m^{-1}\cdot K^{-1}$)	2.5	2.5	2.5	3.0	3.0
Heat Capacity($J\cdot kg^{-1}\cdot K^{-1}$)	1050	1050	1050	1050	1050
Radioactive Heat($W\cdot m^{-3}$)	1×10^{-6}	5×10^{-7}	5×10^{-7}	0	0
Thermal Expansivity(K^{-1})	3.2×10^{-5}	3.2×10^{-5}	3.2×10^{-5}	3.2×10^{-5}	3.2×10^{-5}

From Hirth & Kohlstedt (1996), Ranalli (1995) and Schmalholz et al. (2009)

Figure Captions

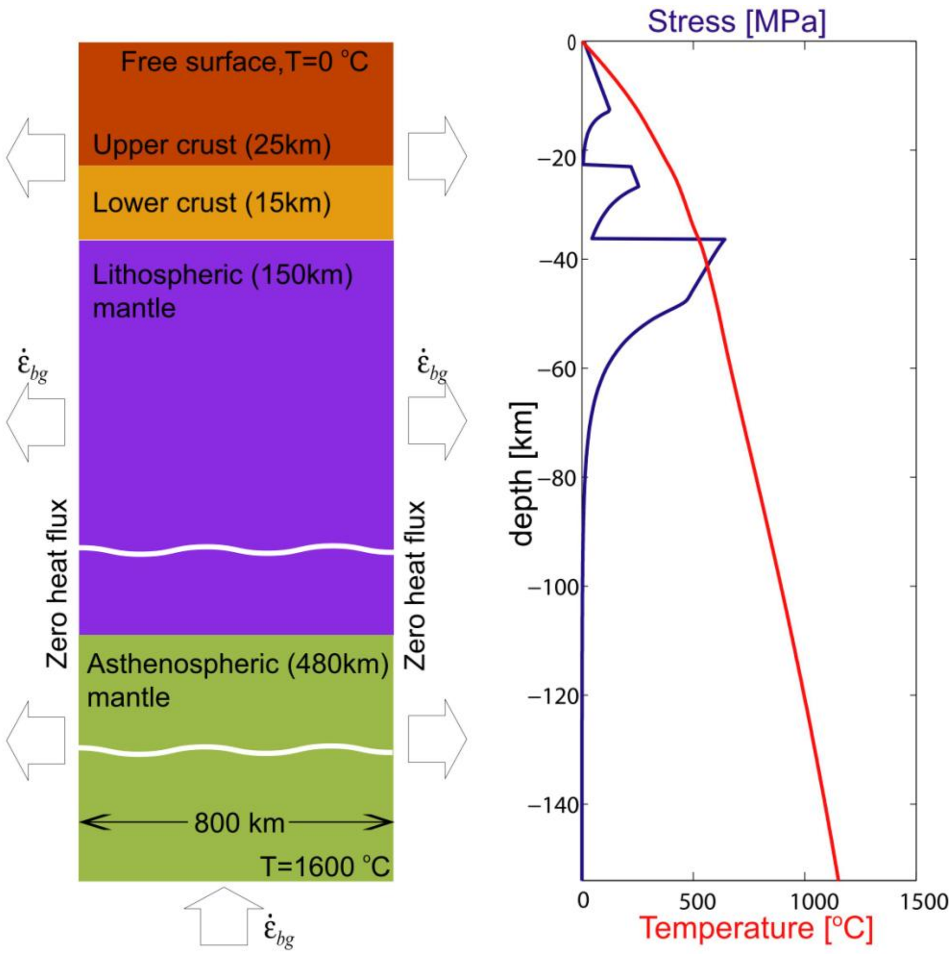

Figure 1.
(Left) Model setup for 2-D simulations. The model consists of an upper crust (25km), a lower crust (15km), a lithospheric (150km) and an asthenospheric (480km) mantle. The whole model has a constant strain rate condition at the bottom and side boundaries, and a free surface boundary condition on the top. Thermal boundary conditions are isotherm at the top (T=0) and bottom (T=1600) boundaries and zero heat flux at side boundaries.
(Right) Illustration of initial temperature and strength profile for the standard model with a thermal age of 500Ma under an extension strain rate of $10^{-14}s^{-1}$. Mohr-Colomb plasticity limits stresses in the crust and whereas Peierls plasticity limits differential stresses in the mantle lithosphere.

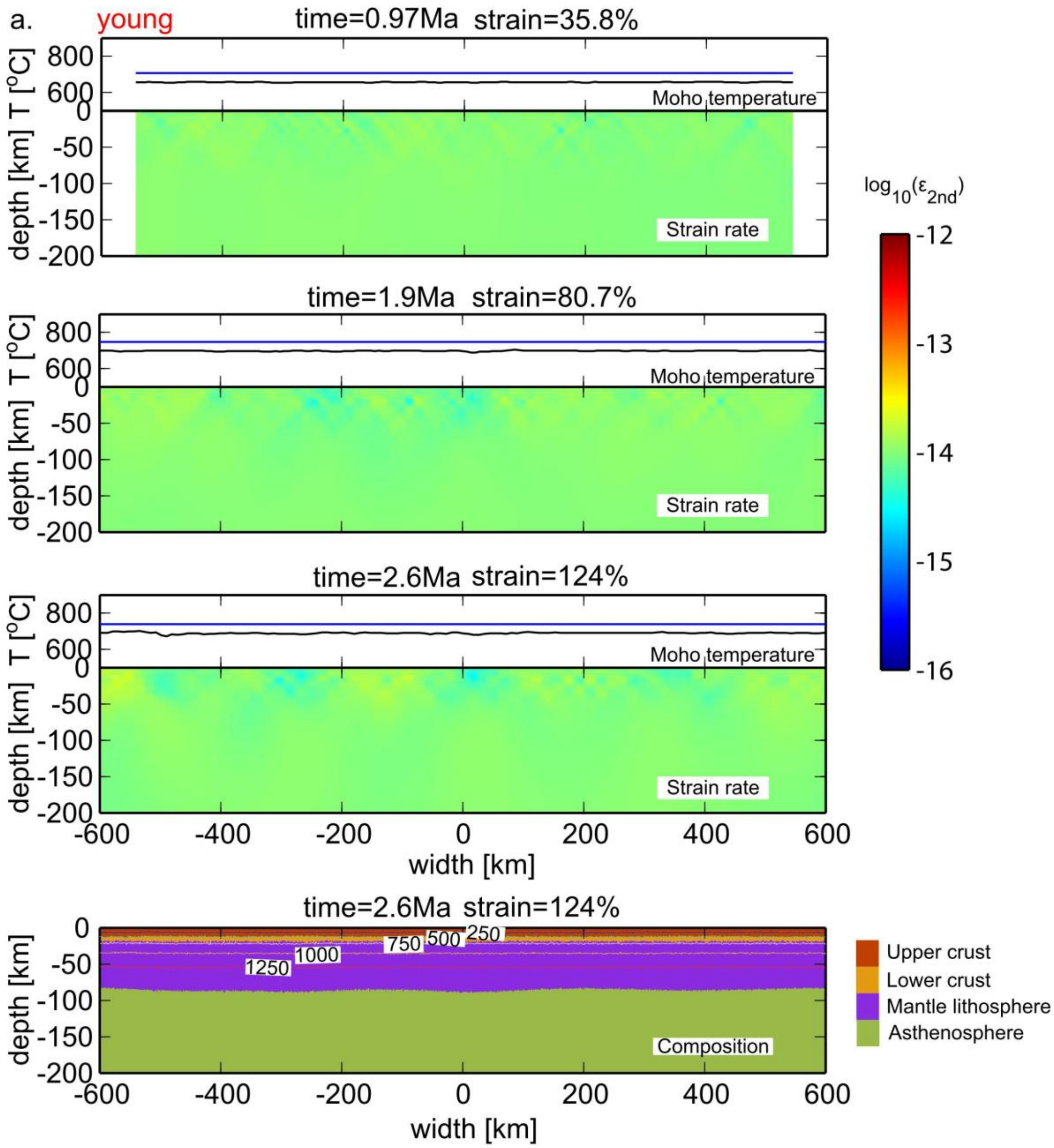

Figure 2. Snapshots of a simulation in the *no localization* mode. The model with a (young) thermal age of 200Ma extends at a strain rate of $10^{-14}s^{-1}$. Strain rate fields at different deformation stages are shown in the first three plots. Moho temperature and a critera (blue line) that indicates the onset of localization if the temperature is locally 50 degrees larger than the average are also shown above each plot of strain rate field. The bottom plot shows the composition field and isotherms.

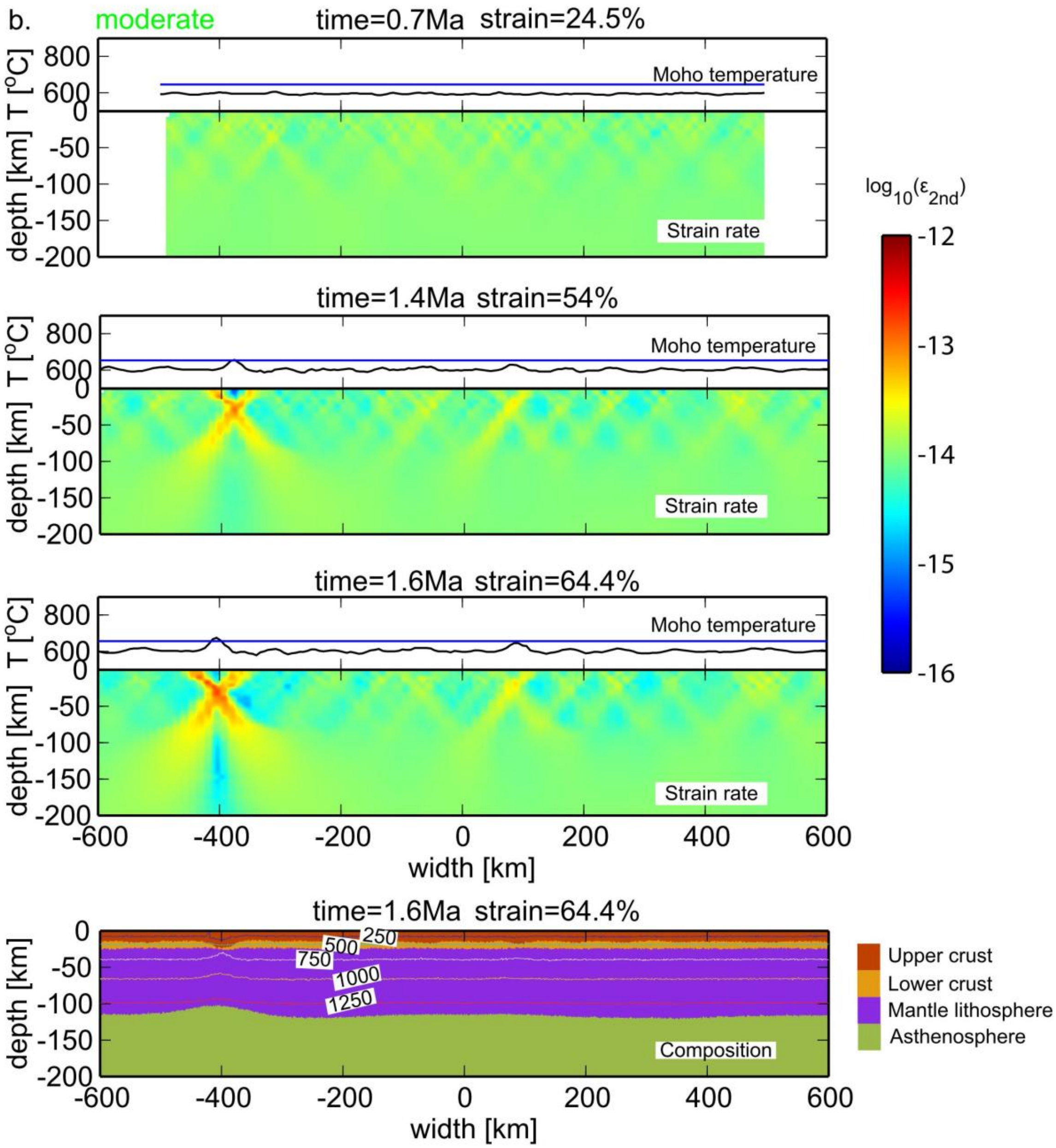

Figure 3. Symmetric localization mode. The model with a (moderate) thermal age of 400Ma extends under the same strain rate as the model of Figure 2. The Moho temperature shows the occurrence of localization, with the composition field indicating that the shear zone is symmetric.

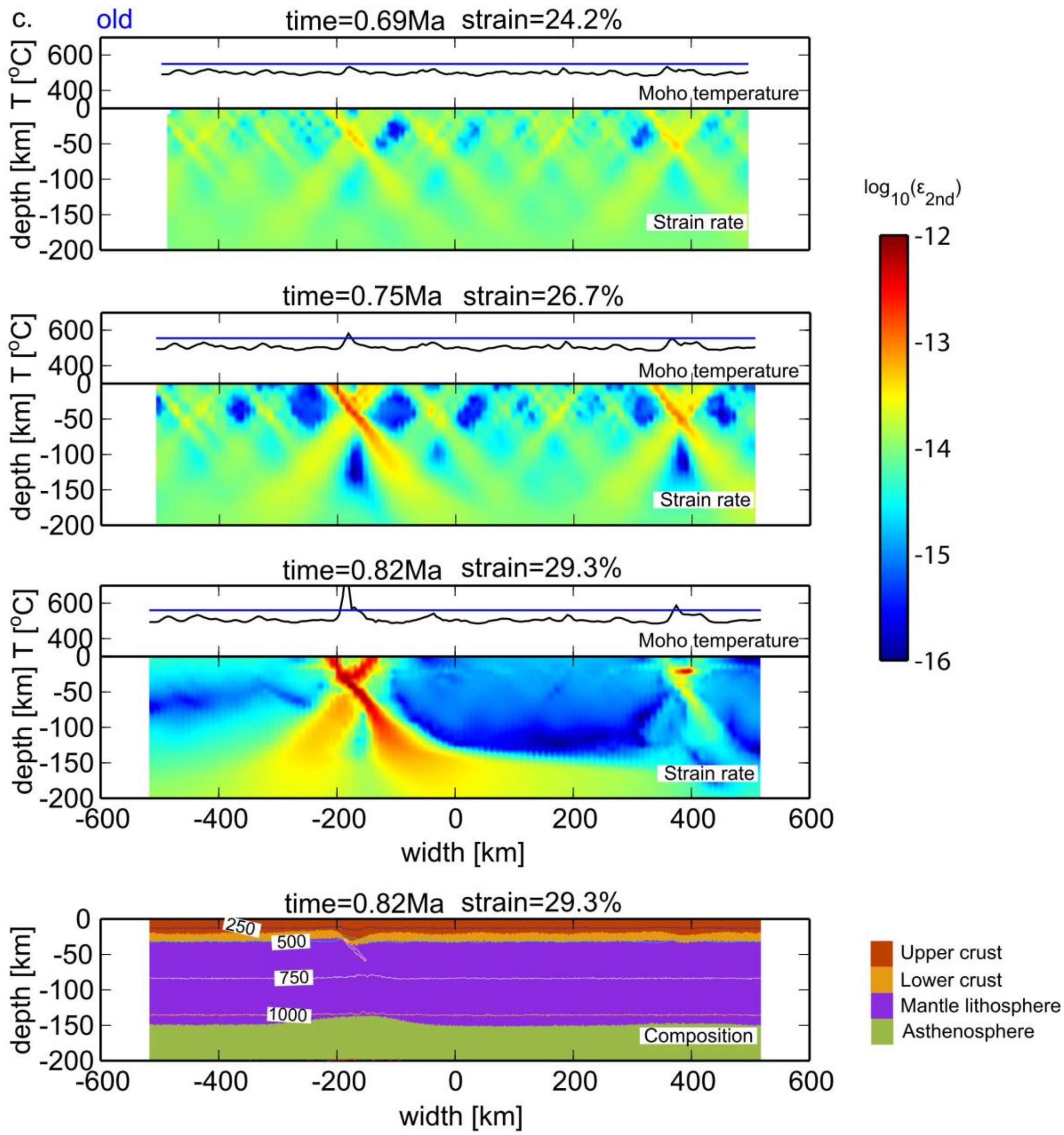

Figure 4. Asymmetric localization mode. Conditions are the same as in the models of Figure 2 and 3, but the thermal age of the lithosphere was increased to 1000Ma. The Moho temperature shows the occurrence of localization, with the composition field indicating that the shear zone is completely asymmetric.

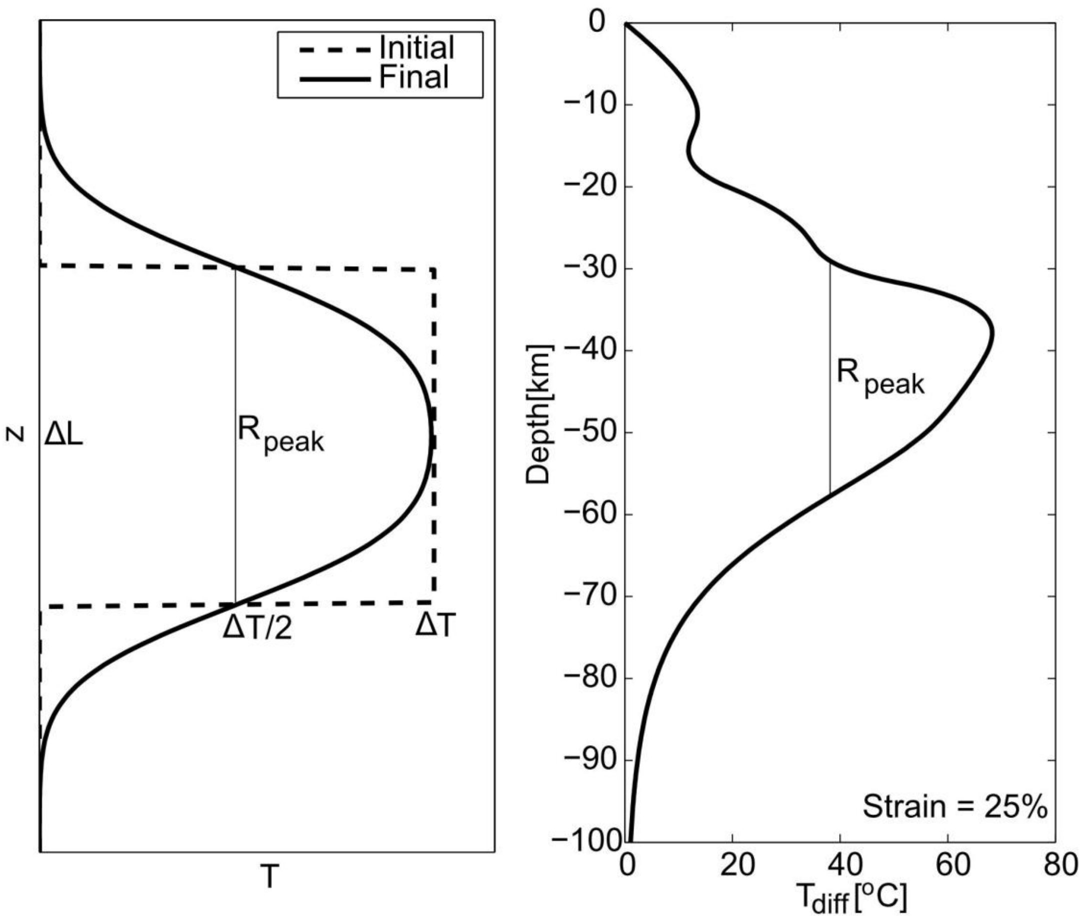

Figure 5. Definition of length scale R. Left) relationship between initial temperature heterogeneity (dash line) and diffused temperature profile (solid line) in a diffusion model. Right) Differential temperature between a 1-D model with and the one without shear heating, with peak width defined.

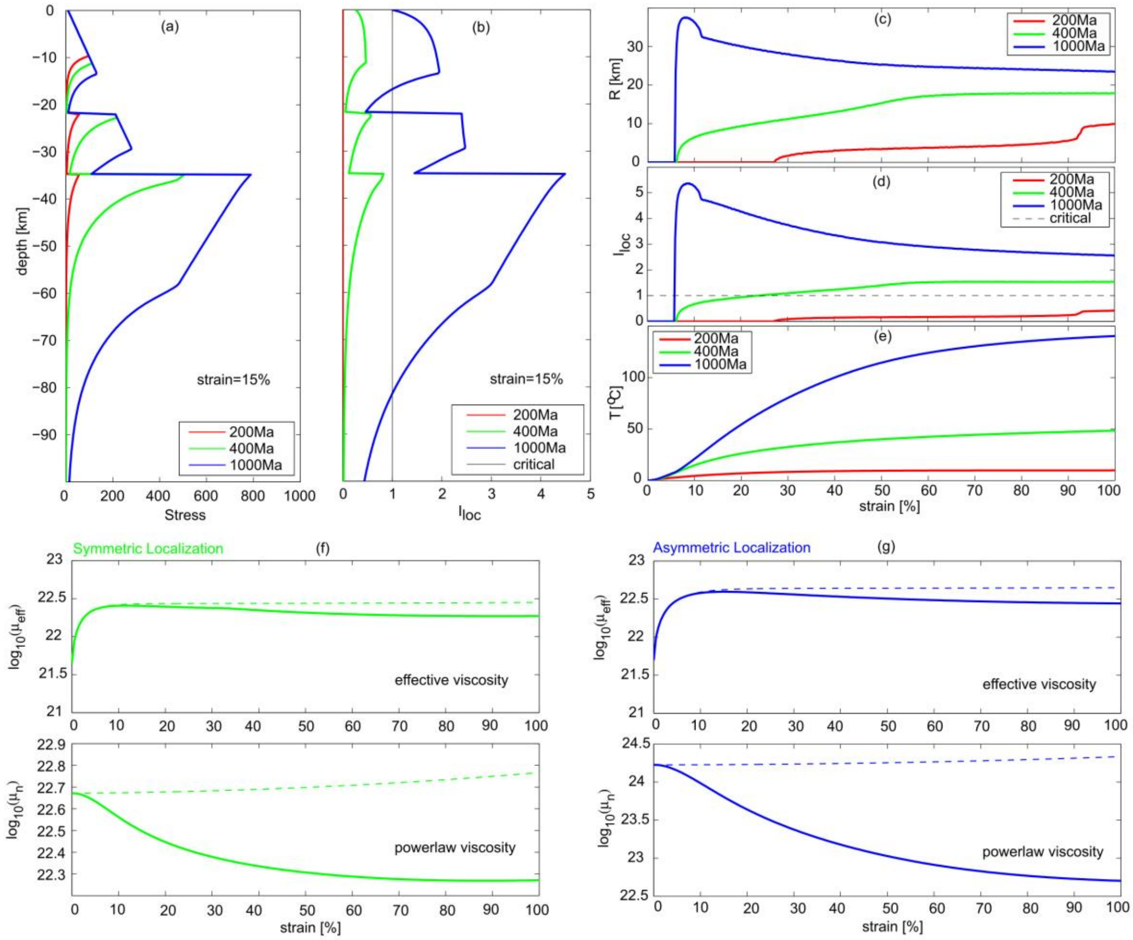

Figure 6. Stress profile (a) and localization number (b) calculated by the semi-analytical model for the setups of Figure 2,3,4 at 15% of total strain. The black line in (b) shows the critical value for the localization number. Evolution of the length scale *R* (c), the localization number I_{loc} (d) and the differential temperature (e) are shown for the setups of Figure 2,3,4. The critical value (dash line in (d)) for the onset of localization is illustrated. (f) and (g) illustrate the effective and power law viscosities (solid lines) for the setups of *symmetric localization* and *asymmetric localization*, respectively. As a comparison, evolutions of viscosities for the same setups but without shear heating are shown as dash lines. In the case of asymmetric localization, the power law viscosity drops by more than an order of magnitude, whereas it is much less for symmetric localization.

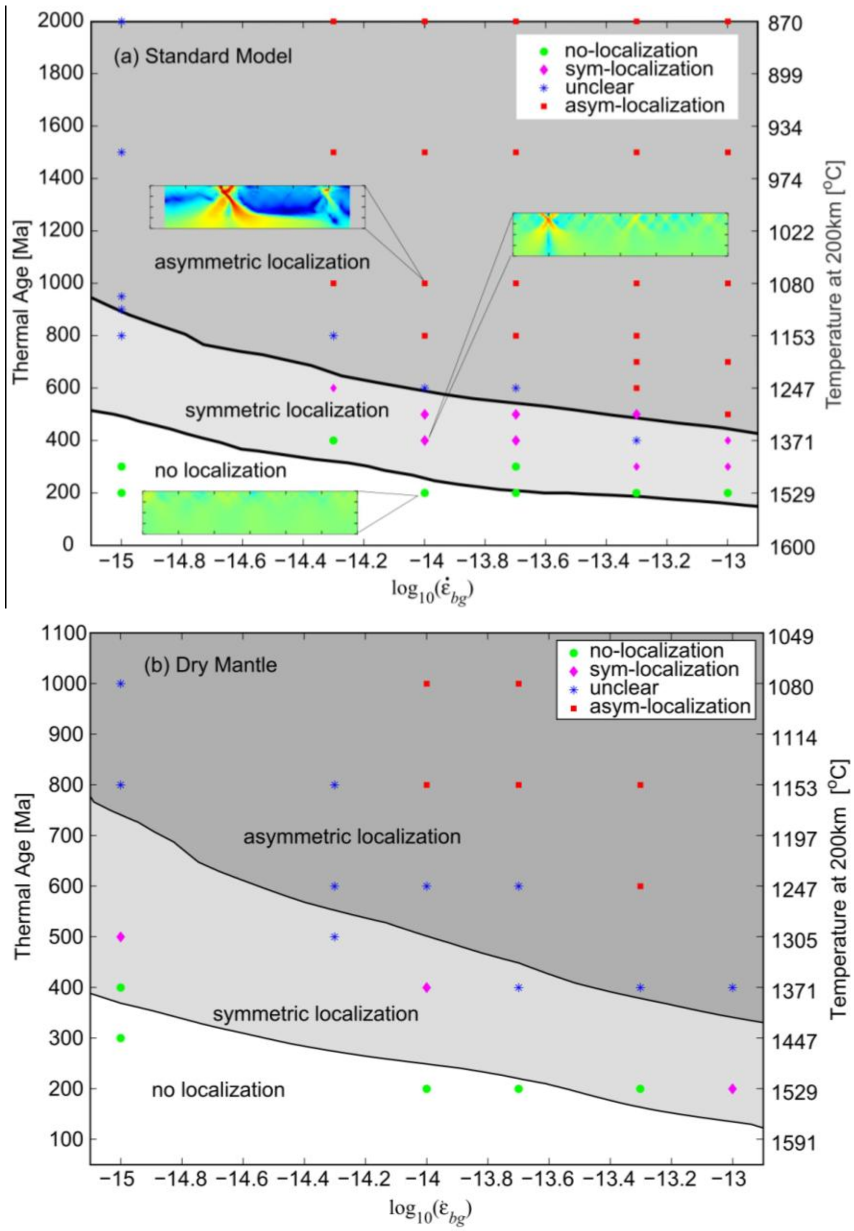

Figure 7. Prediction results of the semi-analytical model for the standard model (a) and the model with dry olivine mantle (b). Data points indicate 2-D simulation results. Insets show three deformation modes for the setups in Figure 2,3 and 4. Temperatures at the depth of 200 km for thermal ages on the left side are shown on the right side respectively.

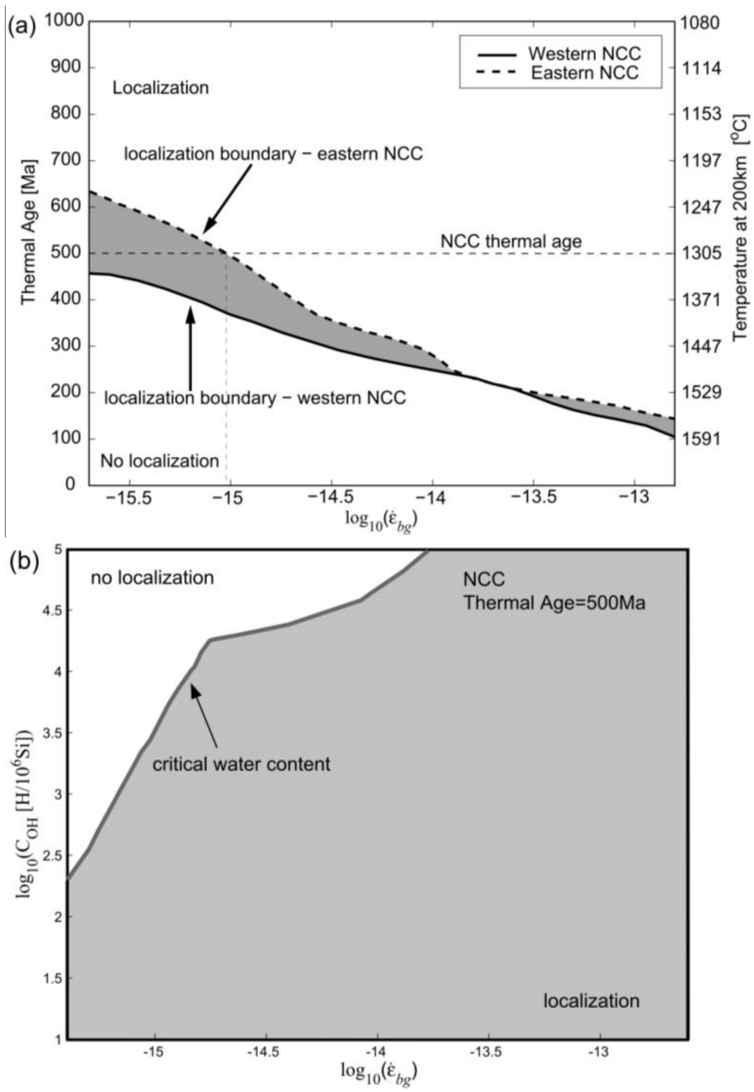

Figure 8. (a) Onset of lithospheric-scale localization applied to the NCC. The solid line indicates the boundary of localization for the western NCC, and the dash line for the eastern NCC. The shading area figures out the parameter space when the western NCC develops localization whereas the eastern NCC doesn't. The mantle in the western NCC is assumed to have a dry olivine mantle rheology, whereas the eastern NCC is wet. (b) Onset of localization versus extension strain rate and water concentration in olivine for the setup of NCC which is assumed to have an initial thermal age of 500 Ma.

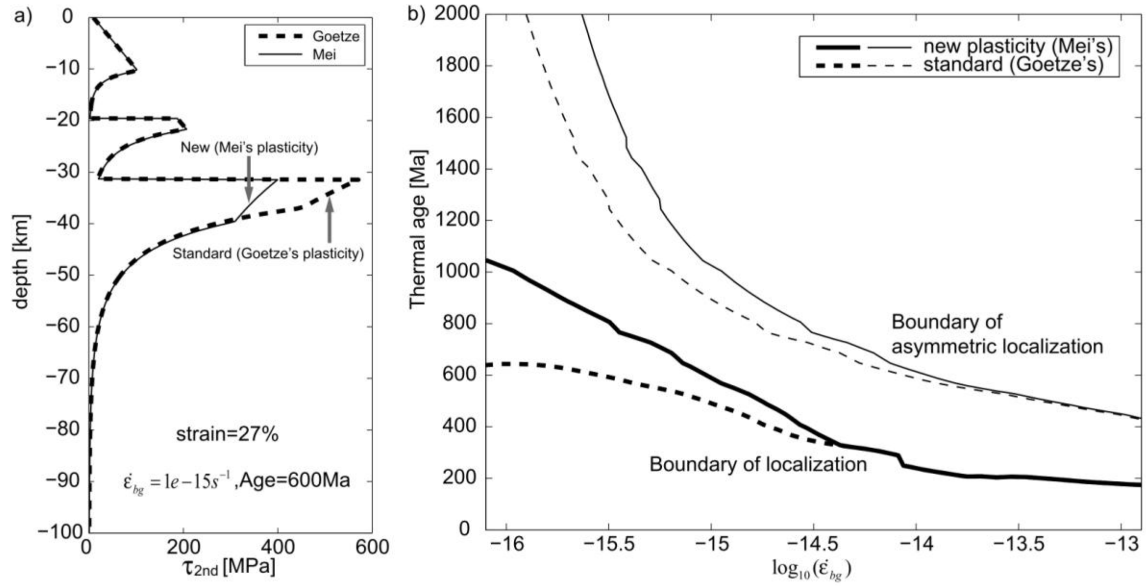

Figure 9.
a) Strength profile shows the Peierls stress by Goetze et al. (dash lines,this study) and the newly derived one by Mei et al. (solid lines) for a background strainrate of $10^{-15}s^{-1}$. b) Prediction of the onset of localization for the Peierls's plasticity by Goetze et al.(dash lines) and Mei et al.(solid lines), respectively.